Characterization of thin LGAD sensors designed for beam monitoring in proton therapy

(Article begins on next page)

14 October 2023

Characterization on beam and in the laboratory of LGAD sensors manufactured at FBK for proton counting in particle therapy

O. A. Marti Villarreal[1,2], G. Peroglio[1], A. Vignati[1,2], S. Giordanengo[2], F. Mas Milian[1,2,3], M. Ferrero[4], L. Menzio[1,2], M. Abujami[1,2], C. Galeone[1,5], O. Hammad Ali[6], M. Centis Vignali[6] , G. Borghi[6], F. Ficorella[6], R. Cirio[1,2], V. Monaco[1,2], R. Sacchi[1,2]

[1]Università degli Studi di Torino, Italy
[2]Istituto Nazionale di Fisica Nucleare (INFN), Sezione di Torino - Torino, Italy
[3]Universidade Estadual de Santa Cruz, Ilhéus, Brazil
[4]Università del Piemonte Orientale, Novara, Italy
[5]GSI Helmholtzzentrum, Darmstadt, Germany
[6]Fondazione Bruno Kessler, Centre of Materials and Microsystems, Trento, Italy
 E-mail: martivil@to.infn.it

Abstract

A fast LGAD sensor prototype was developed by the University and INFN of Torino as an online monitor of the fluence rate of clinical proton beams. The sensor is segmented into 146 strips (114 μm width, 26214 μm length, 180 μm pitch, 2 strips without gain, 144 strips with gain, and a nominal inter-strip distance of 66 μm). Fourteen wafers (xx Epi and xx Si-Si substrate…) were produced by Fondazione Bruno Kessler (FBK, Trento, Italy) in 2020. In this paper, we report the laboratory characterization of sensors performed at the University of Torino and at FBK using a probe station connected with the power devices analyzer for static DC electrical test and the TCT to study dynamic properties. Subsequently, one sensor was tested on a clinical beam at Centro Nazionale di Adroterapia Oncologica (CNAO, Pavia, Italy), together with its custom readout electronics. A percentage of good strips of 87.27 and 99.80 for LGAD and PiN respectively, and a percentage of good sensors of 39.80 (LGAD) and 85.71 (PIN) was found. The average full depletion voltage obtained was ranging between 22.14 and 23.36 V for Si-Si and 34.98 V for Epi wafers. A mean breakdown voltage of about 212 V was found for good sensors measured on the backplane. On a representative subgroup of 16 sensors selected from different wafers, a consistent correlation between the measurements performed at FBK (99.74% yield) and at the University of Torino (99.79% yield) was observed. The measured inter-strip distance was 80.8 μm, 22% larger than the nominal no-gain distance and slightly dependent on the laser intensities. Furthermore, the ratio between 90th and 10th percentiles for the leakage current at 160 V was lower than 1.62 for all cases. The laboratory characterization together with the test data acquired at CNAO showed promising results and prepared the groundwork for future beam tests using the digital channels of the counter prototype.

1. Introduction

The University and INFN of Torino are working on new beam monitors for particle therapy based on segmented Low Gain Avalanche Detectors (LGAD) [1,2]. Nowadays, the monitoring of clinical beams is performed by gas-filled ionization chambers based on real-time integration of the charge produced in the gas by incoming particles. This approach offers several advantages in terms of robustness, transparency to the beam, large sensitive area, and good radiation resistance [3]. Several problems, such as slow collection time, low sensitivity, and dependence on beam energy and environmental parameters [3], limit the use of ionization chambers in the forthcoming advanced delivery techniques, such as fast scanning modalities, which will improve the accuracy and reduce the duration treatments in order to increase the patient throughput [?]. Solid-state detectors could be an ideal alternative for a new generation of beam monitors because they feature fast response (~ns), good time resolution (< 100 ps), and excellent sensitivity able to detect single protons. However, radiation damage and signal pile-up limit their use on high fluxes of therapeutic beams. Ultra-Fast Silicon Detectors (UFSD) are based on LGAD [3, 4] and have a thin 1 micrometer p^+ gain layer implanted under the n++ cathode. As a result, the doping profile is characterized by a large increase in doping concentration in the region close to the n^{++}/p^+ junction, resulting in a local increase of the

---

[1]https://www.technoprobe.com/
[2]https://www.prusa3d.com/category/original-prusa-i3-mk3s/
[3]http://particulars.si

electrical field (around 300 kV/cm). This creates electron/hole avalanche multiplication for the electron and less extend to holes leading to a signal enhancement with a similar noise level of a traditional silicon sensor of the same geometry [4, 5]. In 2020, Fondazione Bruno Kessler (FBK, Trento, Italy) delivered a production entirely dedicated to a sensor prototype specifically designed to online monitor the fluence rate of proton beams, i.e. a particle counter sensor [6]. This prototype is segmented in strips to reduce the expected particle rate per channel and therefore pile-up in each strip, and allows covering a great sensitive area (2.6 x 2.6 cm^2). The full characterization of the counter prototype in the laboratory and a preliminary test performed at Centro Nazionale di Adroterapia Oncologica (CNAO, Pavia, Italy) on a clinical proton beam will be reported and discussed in detail.

2. MoVEIT 2020 FBK's production

A production dedicated to the counter prototype was designed and manufactured by FBK. In each wafer 8 sensors are present (hereinafter defined *big sensors or A_N*), as shown in Fig. 1. Each A_N consists of a large sensitive area of 2.6 cm by 2.6 cm (Fig. 2a) conceived to cover the entire clinical proton beam spot () and it is segmented in 146 strips (114 μm by 26214 μm and a pitch of 180 μm). Seven (out of the 8 available) A_N structures feature two strips (1,2) without gain layer, i.e. they are conventional PiN diodes, while the remaining ones (from strip 3 to146) have a gain layer (A_1, A_2, A_4, A_5, A_6, A_7, and A_8), as shown in Fig. 2b

The remaining big sensor (A_3) has 146 strips without the implantation of the gain layer. The term PIN diode refers to a structure composed of a sequence of p/i/n silicon. Standard silicon sensors are often called PIN diode, even though the bulk is not made of intrinsic silicon but is lightly doped [4].
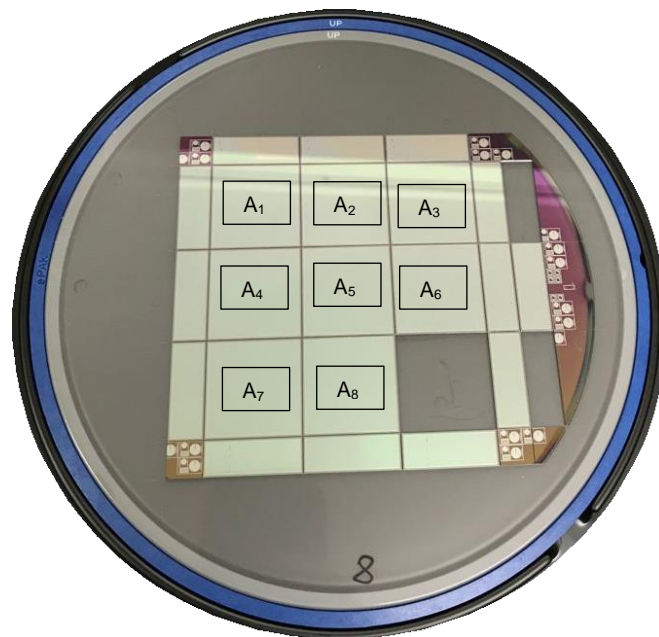

Figure 1.

The structures of this production are based on the design described in [5]. A simplified cross-section not-to-scale of one LGAD is shown in Fig. 2c. The p-stop is a high p-type doped (?) material [4,7] surrounding each strip and its objective is to electrically isolate two neighboring strips from (?) the inversion layer created by positive charges at the Si-SiO$_2$ interface. The p-stop thus adds a no gain region, affecting the fill factor [8]. The gain-gain distance between two neighboring strips (super-safe designed) is 66 um. The gain layer is a p$^+$ material with a doping concentration of $\sim 10^{16}$ /cm^3, with a thickness of $\sim$ 1 μm able to create an electric field large enough to activate electrons' charge multiplication. The gain layer is implanted under the n^{++} cathode separately for the shallow gain implants by a small distance of less than 1 μm. The

JTE or n-deep surrounds the gain layer and collects the electron/hole generated in the inter-strip region, controls the junction curvature and reduce the electric field at the border [8]. In the absence of this structure, particles hitting the sensor in the inter-strip region would generate a delayed signal due to the higher distance from the collecting electrode [4,7]. One or more Guard Ring (GR), i.e. implants made of high n-type doped material, are placed on the edge of the detector. They are floating except the first one as shown in Fig 2.b, which is biased at the same potential as the strips). GRs avoid early breakdown at the periphery of the detector [4,7], collecting the charge carriers generated outside of the strip (Fig 2.b).

Besides the big sensors A_N, there are 3 additional detectors with 1/3 the total area of the A_N and several strips with different dimensions, designed for laboratory testing purposes, and XX small detectors (not shown in Fig. 1) designed for timing applications [9,10]. Those sensors are covered by the entire beam spot and have 11 strips (10 with Gain, 1 without Gain), each characterized by a sensitive area of 2.2 mm^2.
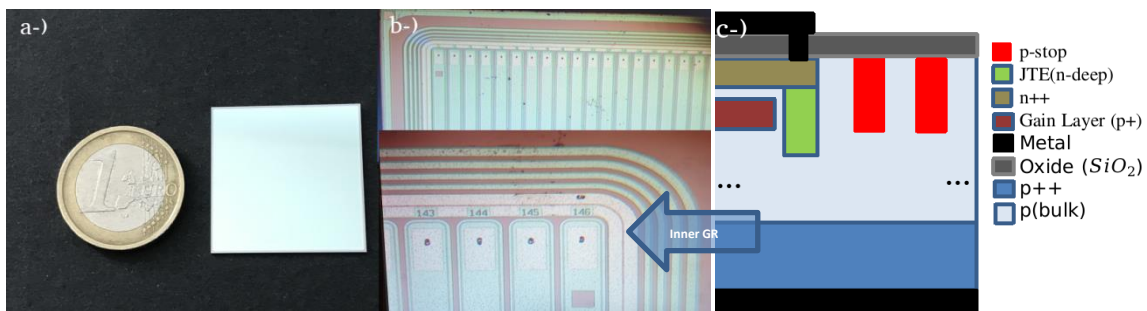

Figure 2.

In all 14 wafers, which can be grouped into three classes (Table 1), boron was the acceptor dopant used for the gain layer implant. It was enriched with a dose of carbon in order to improve the radiation resistance equal to C_1/C_A (Arbitrary units) [4,5]. It is important to point out that the carbon has been deposited only in the gain layer to avoid an acute increase in the leakage current. The gain layer (Boron-Low-Diffusion) enriched with this dose of carbon is the most radiation hard design reaching 80% of the active fraction of the gain layer at a fluence of $1.5*10^{15}$ neq/cm^2 which are equivalent to one year of clinical proton irradiation in a single treatment line [10].

Two different substrates were used: Epitaxial silicon layer (Epi) with an active thickness of 45 μm for wafers 1, 2, and 14, and Si-Si with an active thickness of 60 μm for the remaining wafers. Additionally, two doses of boron in the gain implant are used, as shown in Table 1, where the reduction of gain layer doping concentration that occurs when is enriching this layer with carbon was considered for selecting the doses. Details about the fabrication of silicon LGAD sensors based are described by Giacomini [11].

Group	Wafer n.	Dopant	Substrate	Dose P_{gain} (a.u)	Carbon	Diffusion	d (μm)
A	1,2, 14	Boron	Epi	0.96	C_1/C_A	B-LD	45
B	3,4,5,6,7	Boron	Si-Si	0.98	C_1/C_A	B-LD	60
C	8,9,10,11,12,13	Boron	Si-Si	0.98	C_1/C_A	B-LD	60

Table 1.

3. Laboratory characterization

Measurements were performed at the Laboratory of Innovative Silicon Sensors of the University and INFN of Torino and at FBK. The experimental setups will be described in detail in the following subsections.

3.1. Static characterization of LGAD sensors (current-voltage)

Two different experimental setups were used for measuring I(V) curves and will be described in the following.

[1]https://www.technoprobe.com/
[2]https://www.prusa3d.com/category/original-prusa-i3-mk3s/
[3]http://particulars.si

a) Switching Matrix and dedicated probe card

Since the big sensor has a large number of strips (146), a multi-strip configuration was used (Fig. 3). A custom probe card with 40 needles (with 180 um distance between needles, as the pitch of the sensor) for contacting the strips and grounding the GR was designed and produced by Technoprobe[1]. The interconnection between the Power Device Analyzer (Keysight B1505A) and the probe card was performed through the Keithley 7002 Switch System equipped with four 7058 low current scanner cards (ten per channels). The Device Under Test (DUT) is placed on top of the chuck, which is connected to the Power Device Analyzer through the High Level (-V) of the High Voltage Source Monitor Unit B1513C (HV-SMU). The Low Level (0 V) of this module was connected directly to the GR using the respective needle of the probe card. The other needles of the probe card were used to contact the strips and were connected to the Medium Power Source Unit B1511B (MP-SMU) using the matrix unit, which allows selecting which strips on the detectors are measured and ground it.
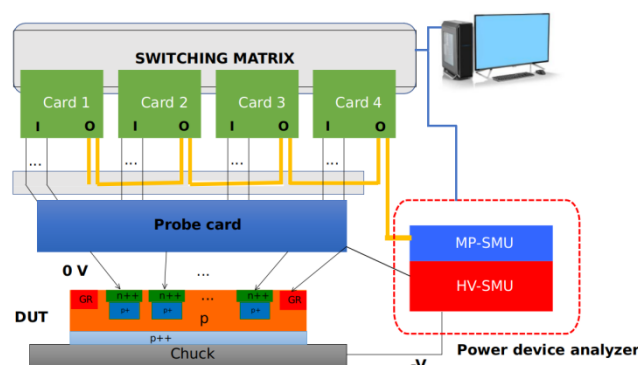

Figure 3.

With this scheme, only 40/146 strips can be measured simultaneously. (We were able to measure 24 strips, but the remaining 16 strips were grounded). The remaining strips(106) were left floating.

b) Conductive polymer: "Elastomer"

The second setup consists of a conductive polymer (Elastomer) [12]. With this experimental scheme, all strips were measured at once. Given the size of each strip opening (200 μm $\times$104 μm), the positioning procedure of the elastomer on top of the strips' openings might leave some strips floating. In the future, increasing the elastomer dimension could be considered to solve this issue, paying attention not to damage the surface of the sensors. The positioning procedure can be visualized in Fig. 4 and numbered as follows.

1-) A piece of elastomer is cut with the same size of the strips opening;
2.3-) A maskcap with the same dimension of the detector was designed using 3D AutoCAD 2020 and printed using a 3D printer model (ORIGINAL PRUSA i3 MK3)[2];
3.4-) A copper tape was inserted around the perpendicular surface of the cap. The mask covers the entire detector. The cap is then placed on top of the mask and a "crocodile clip" contacts the conductive tape, the elastomer, and the strips + GR of the DUT. In this approach, the detector is biased using the chuck connected to the power device analyzer through the High Level (-V) of the HV-SMU, and the Low Level (0 V) of the MP-SMU using a "crocodile clip";
5-) Finally, we put a block of lead in order to make good contact between the conductive tape, the elastomer, and the sensor.

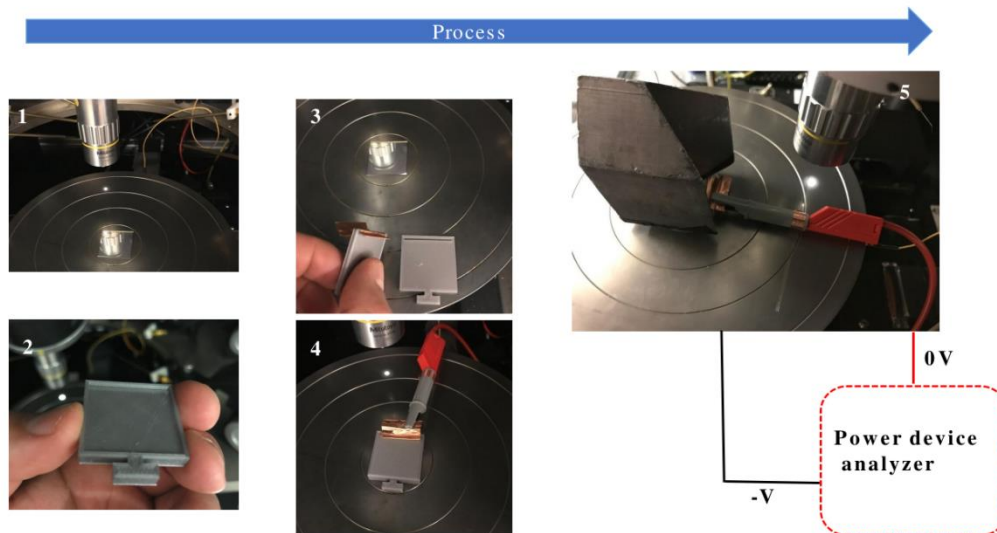[1]https://www.technoprobe.com/
[2]https://www.prusa3d.com/category/original-prusa-i3-mk3s/
[3]http://particulars.si

Figure 4.

3.1.1. I(V) Analysis

An automatic algorithm to extract the I(V) curves parameters was implemented in Matlab R2021a.

The I(V) characteristics are performed using the experimental setup explained in sections 3.1. This measure allows achieving one of the more relevant analyses that can be done on silicon sensor technology examining the reverse bias region. It is considered the fingerprints for the semiconductor device because it carries the main characteristics of the detectors, and in practice, manufacturing problems cause a deviation from the expected shape of the curve.

An example of the I(V) curves measured on 144 LGAD strips at room temperature for wafer 3, sensor A2, is shown in Fig 5. Fig 5a. shows the leakage current vs. bias voltage for each strip independently, while Fig 5b. shows the total current vs. bias voltage. The total current is measured on the backplane using the High Voltage Module and it defines the working point of the DUT. It has a compliance which is the maximum current provided by the Power Device Analyzer and blocks the over exponential growth of the leakage current to protect the DUT.

The y-axis of Fig. 5a is reported in logarithmic scale. Three different regions are observed:

1-) From 0 V to -24 V;
2- From -24 V to -200 V;
3-) From -200 V to -275 V;

Three main regions can be distinguished depending on the voltage values: the full depletion of the active volume of the sensors [0; -24 V], the exponential trend ($\sim e^{k(V_{bias})}$) due to the effect of the gain layer, where k is proportional to the sensor gain [-24V; -200V], the breakdown of the sensor [-200; -275]. As shown in Fig. 5a, the first strip (green curve) features breakdown around -200 V, which is the same bias voltage observed in Fig. 5b for the total current. Thus, this detector cannot be used with a bias voltage higher than -200 V.
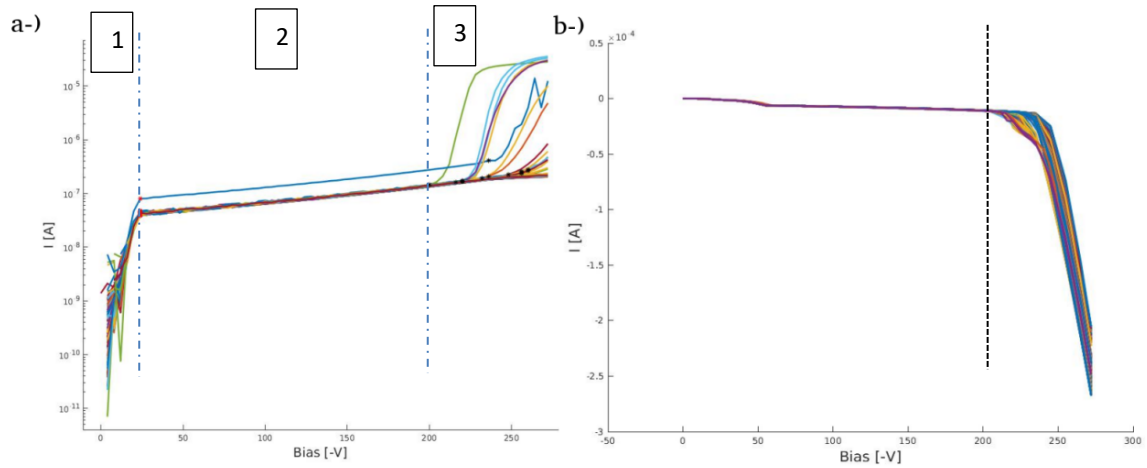
Figure 5.

The automatic method for the extraction of the I(V) characteristics of each strip is based on the numerical derivative, after smoothing the data with moving average. The depletion voltage is defined as the first bias voltage value following the derivative minimum, as shown in blue in Fig. 6 (-24 V). This method has a systematic error of 4 V due to the voltage step used during the measurements.
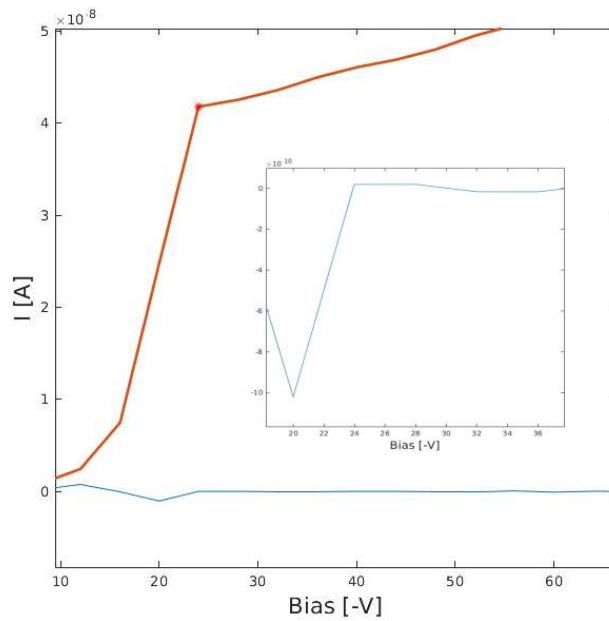

Figure 6.

After the depletion region of the curve, the exponential trend is due to the charge multiplication. The following modification to the leakage current was applied:

$$I' = Ln(I(V_{FD}:end)) \; or \; Ln(-I(V_{V_{GR}}:end)) \quad (1)$$

A linear fit was performed to the data from the full depletion voltage (V_{FD}) or depletion voltage of the GR ($V_{V_{GR}}$) up to the last bias voltage measured. The general method adopted for finding the breakdown voltage for a single strip is explained. The same procedure is applied to calculate the breakdown voltage on the backplane using the total current. The only difference is, as shown in Eq. 1 right: the inversion of the total current and the looking point is from the depletion voltage of the Guard Ring, up to the last bias voltage measured. Then, a coefficient of determination (R^2) < 0.97 was used to find the strips with breakdown, once they were

[1]https://www.technoprobe.com/
[2]https://www.prusa3d.com/category/original-prusa-i3-mk3s/
[3]http://particulars.si

identified. Two additional criteria were applied to determine the exact point of breakdown, as follows.

First Criterion. Using the adimensional function K(I,V) [13,14]:

$$K(I, V) = \frac{\Delta I}{\Delta V} \frac{V}{I(V)} \quad (10)$$

where: I(V) is the leakage current for a specific bias voltage, V the applied bias voltage, and $\frac{\Delta I}{\Delta V}$ the I(V) curve's slope, the breakdown voltage was defined as the last bias at which $K(I, V) < 8$ [14].

*Second Criterion (*reinforced one). Whenever criterion 1 fails, it defines the first bias voltage where the strip reaches compliance.

3.2. Static characterization of LGAD sensors (capacitance-frequency, and capacitance-voltage)

Fig. 7 shows the experimental setup used to measure the C(f) and C(V) curves. The DUT is placed over the chuck. The Power device analyzer model Keysight B1505A was used with the High Voltage Source Monitor Unit B1513C (HVSMU) and Multi-Frequency Capacitance Measurement Unit Module B1520A (MFCMU) modules, using a Bias Tees to get as input the DC bias from the High Voltage Module and a Sinusoidal wave (AC signal) from the MFCMU. The sum of these two input signals is split in Low Level (0 V) and High Level (-V). Superimposing a small sinusoidal voltage to the DC bias allows measuring the capacitive behavior of the detectors, which strongly depends on the frequency used. The overall sensor impedance is then described by taking into account the ohmic and capacitive parts as shown in Eq. 2. Then, the DUT is biased using the chuck and the needles of the manipulators, which receive the High Level and the Low Level, respectively. In this scheme, the neighboring strips and the GR were short circuited to the ground using additional manipulators. These tests are meant to study the gain layer doping concentration, gain layer depth, gain layer depletion voltage, full sensor depletion voltage and the response of the sensors for different AC frequencies.
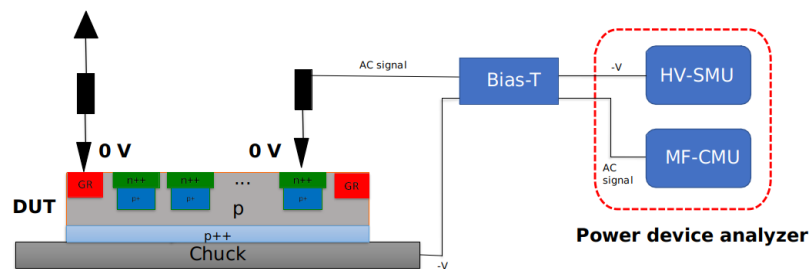

Figure 7.

The electrical response in a plane silicon sensor can be modeled using a capacitor-resistor in parallel. This is also the case for unirradiated LGAD sensors [4,5,7]. Therefore, the capacitance is taken from the imaginary part of the admittance, as shown in Eq. 2.

$$Y = G(\omega) + jB(\omega) = \frac{1}{R_p} + j\omega C_p \quad (2)$$

This model was considered for the laboratory measurements and the quantities were directly measured selecting the "Cp-Rp model" in the Power Device Analyzer. A C(f) scan is first performed to find the optimal frequency of the AC signal, by setting a bias voltage able to partially deplete the gain layer. In this condition, the capacitance has a great value and almost

[1]https://www.technoprobe.com/
[2]https://www.prusa3d.com/category/original-prusa-i3-mk3s/
[3]http://particulars.si

constant before his drop [4,7]. It depends on the characteristics of the sensors and measurements conditions. After that, with the proper frequency, the C(V) can be performed.

3.2.1 C(V) Analysis

The C(V) characteristics were carried out using the experimental setup described in 3.2. When the reverse bias voltage is applied, the depletion starts in the n^{++}/p^+ junction, due to the high doping concentration of the gain layer ($\sim 10^{16}/cm^3$), and around 20 Volts are necessary to deplete it. The depletion region is then extended to the p^{bulk}. Because of the high resistivity of the p^{bulk}, few Volts are necessary to fully deplete it. The C(V) curves of a PiN diode and an LGAD coming from the same wafer show the same capacitance after the full depletion voltage, and this happens because the sensors can be approximated to parallel plate capacitors [15]. The gain layer depletion voltage is ideally found using the numerical second derivative (D_2) approach in the region of interest (Fig. 8b). It is the point shown as a black point in Fig. 8b. Observing the C(V) or 1/C(V)^2 (Fig. 8a) it is possible to identify when sensors are fully depleted, i.e. the region when the C(V) or 1/C(V)^2 is almost constant and the value of the second derivative is almost 0, as shown in Fig. 8b. Therefore, the fully depletion point is found using the following criteria:

1-) the second negative spike in D_2 (see Fig. 8b);
2-) Starting at this point to the end of the array of values of D_2, look at the exact point when D_2(i)*D_2(i-1) <=0;
3-) The full depletion voltage is shown in Fig 8b as a red point mark.

It is important to remark that this method has a systematic error due to the step used for the sweep in the measurements of 0.2 V. The acceptor doping concentration vs. depth was calculated using the procedure explained in detail in [4,5,7].
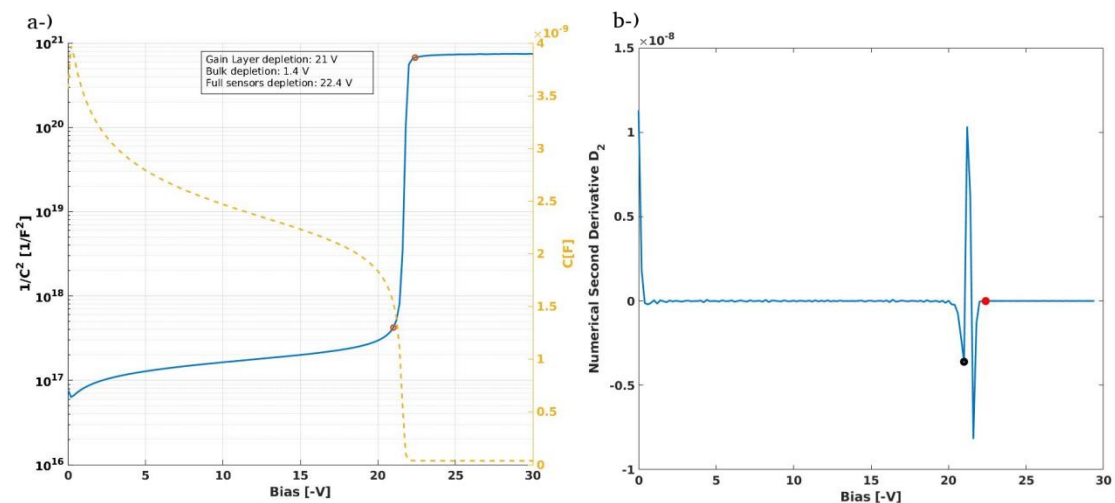

Figure 8.

3.3. Transient current technique (TCT) system

The Transient Current Technique (TCT) setup was developed by Particulars[3] in Ljubjana (Slovenia). The signal is induced into the detectors by using an infrared picoseconds laser with a wavelength of 1064 nm, simulating the passage of a Minimum Ionizing Particle (MIP). The laser was split in two: 89.5 % going to the reference diode to control the laser intensities and fluctuations, and 10.5 % going to the sensor. The detectors Type E (Fig. 1, bottom) were glued on a PCB board designed by the electronics laboratory of the INFN Torino. The negative bias voltage was supplied to the device's backplane, while strips 5 and 6 were wire-bonded to the output connectors of the board. Two low-noise current amplifiers (CIVIDEC Broadband amplifiers, 20 dB) received as input the signals from the board and were readout by a Lecroy

[1]https://www.technoprobe.com/
[2]https://www.prusa3d.com/category/original-prusa-i3-mk3s/
[3]http://particulars.si

Oscilloscope (740Zi, 40 GSample/s). An xyz-stage control with sub-um precision was used to scan the optical window.

4. Beam Test

Two good sensors from wafers 1 and 14 were selected for being tested with a clinical beam. Each sensor was glued on a PCB board hosting 6 ABACUS chips. The ABACUS chip [6], specifically design for the counter prototype, has 24 channels, etc… The signals out of the chips are acquired by an FPGA…. (Fig. 9). The first sensor ("A", W14-A4) was placed at the isocenter and the second one ("B", W1-A4) was placed at 470 ± 1 mm from "A". All channels of the sensor A were readout, while only the two analog channels present on the board's edge were used for reading out strip 1 and 146 of sensor B. The preliminary results and the experimental setup for board "B" are reported in detail in this paper.
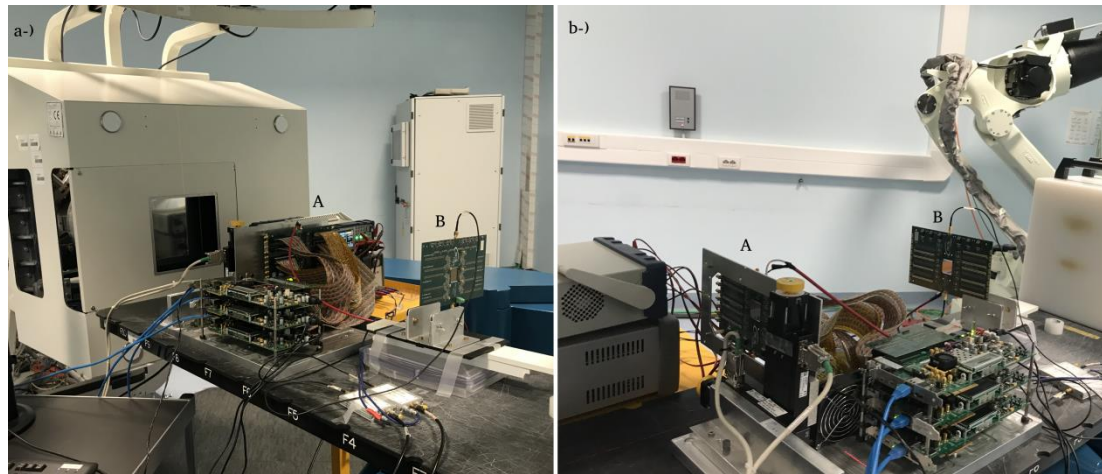

Figure 9.

Two low-noise current amplifiers (CIVIDEC Broadband amplifiers, 40 dB) were connected to the analog outputs of the board and were then acquired through the high rate digitizer CAEN DT5742 (5 GS/s, 12 bits resolution, 1 ADC = 0.24 mV, acquisition windows of 1024 samples, i.e. 204.5 ns). A PC connected to the digitizer with an 80 MB/s optical link was used to control the acquisition, collect the waveforms for the offline analysis, and produce an asynchronous software trigger when the previous events were stored in memory.

5. Results and Discussion

5.1. Production Yield and Wafer Uniformity

The production yield and wafer uniformity were measured at FBK. The experimental setup was similar to the one in section 3.1 a) and was performed at 24 C. The entire production was tested: 112 detectors and 16352 strips. A bad strip was defined if it cannot reach 160 V or has more than 0.5 µA at 160 V. Good sensor are those without bad strips. The measured leakage current at 160 V for good LGAD strips is shown in Fig. 10 and the values obtained from the Gaussian fit are reported in Table 2. In order to evaluate the uniformity (U), the ratio between the 90th and the 10th percentiles (90/10) was used. The results were grouped by wafers similarities. The distribution for all the cases follows the Gaussian distribution in which the coefficient of determination was higher than 85 %..

General model Gauss1:	$a_1 \ast \exp(-((x-b_1)/c_1)^2)$				
Wafer n.	a1	b1	c1	R^2	U
1,2, 14 (Group A)	792.4	1.263e-07	3.258e-08	0.95	1.62
3,4,5,6,7 (Group B)	1886	1.235e-07	1.757e-08	0.99	1.30
9 (Group C)	107.1	3.265e-07	7.071e-08	0.85	1.46
8,10,11,12,13 (Group C)	978.3	1.548e-07	3.985e-08	0.97	1.55

Table 2.

Wafer 9 has a different behavior in respect to the other wafers of group C, as its mean leakage current is 2.1 times larger than the other wafers. The first suspicion for this results is a systematic error like the temperature in which was performed the measured, once the leakage current has a strong dependence upon the temperature. Further investigation in the next sections was carried out in Group C to understand such differences.
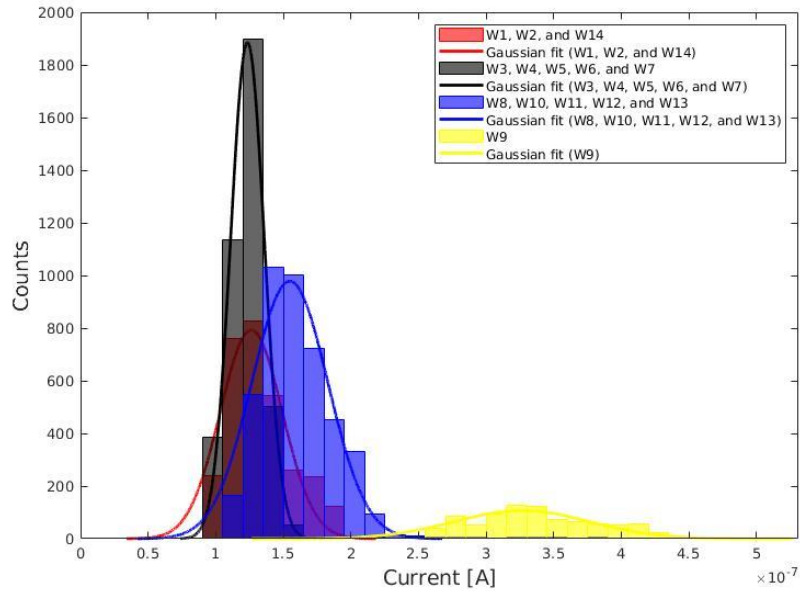

Figure 10. Current distribution at 160 V for good LGAD strip

A value of U lower than 1.62 for all the cases was found, showing a good uniformity. Table 3 summarizes the percentage of good strips and sensors for the whole production. It was observed a percentage of good strips of 87.3 and 39.8 for LGAD and PiN respectively, and a percentage of 99.8 (LGAD) and 85.7 (PiN) of good sensors. As expected, the yield for LGAD sensors is lower than for PiN sensors for all the cases. This happens due to the gain layer's presence, which worsens the yield [15]. In total, of the 112 detectors measured, 51 were good sensors (45.54 %). It is important to point out that even the relatively low yield is expected considering the large area of the detectors [15].

No sensor A3							
Wafer n.	Total strip	Bad strip	Good strip	% Good Strips	Total Sensors	Good Sensors	% Good Sensors
1,2, 14	3066	18	3048	99.41	21	14	66.67
3,4,5,6,7	5110	1024	4086	79.96	35	11	31.43
8,9,10,11,12,13	6132	780	5352	87.28	42	14	33.33
Total	14308	1822	12486	87.27	98	39	39.80
Sensor A3 (No Gain)							
Wafer n.	Total strip	Bad strip	Good strip	% Good Strips	Total Sensors	Good Sensors	% Good Sensors
1,2, 14	438	2	436	99.54	3	2	66.67
3,4,5,6,7	730	2	728	99.73	5	4	80.00
8,9,10,11,12,13	876	0	876	100	6	6	100.00
Total	2044	4	2040	99.80	14	12	85.71

Table 3.

group	Wafer n.	n. strip		Bad strip		Good strip		% Good Strips	Total Sensors	Good Sensors	% Good Sensors
		gain	No gain	gain	No gain		No gain				
A	1,2, 14	3066	438	18	2			99.41	21	14	66.67
B	3-7	5110	730	1024	2			79.96	35	11	31.43
C	8-13	6132	876	780	0			87.28	42	14	33.33
Total		14308	2044	12486	4			87.27	98	39	39.80

5.2. Full Depletion Voltage, Breakdown Voltage and Comparison with the FBK measurements.

The full depletion voltage and the breakdown voltage were measured in the Laboratory of Innovative Silicon Sensors of the University and INFN of Torino using the experimental setup described in 3.1. Fig. 11 shows the depletion voltage found for the entire production, measured as described in 3.1.1.
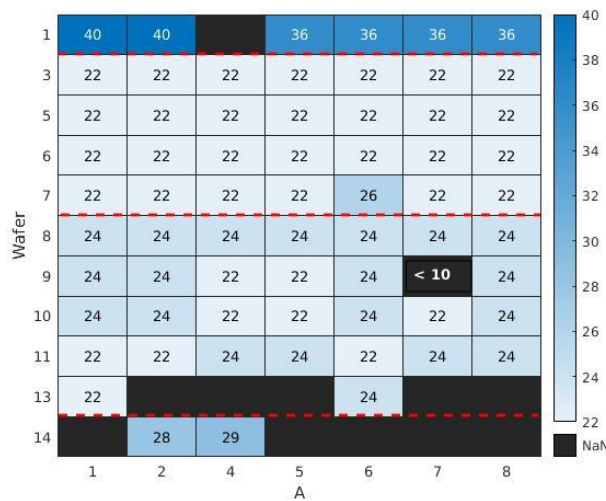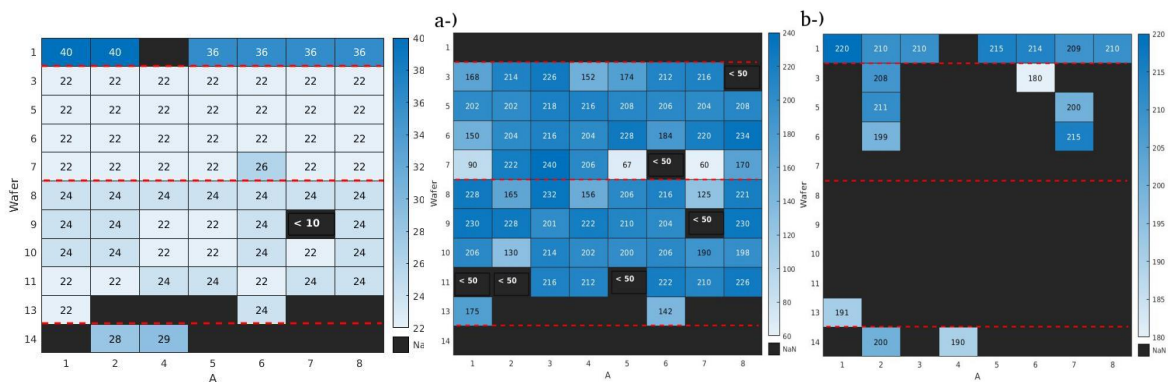

Figure 11.

It is worth noting that exists a systematic error associated with the step used in the measurements. In this case, when was used the elastomer (Group B, Group C), the error was 2 V instead for the setup using the probe card (Group A), the error increased to 4 V.. As we can glimpse, it was used two different experimental setups. This decision was because the total thickness of Group A is different from Group B and C (615 μm for Group A and 630 μm for

Group B and C). This small difference made it difficult to use the same 3D mask to cover the sensors' surface to perform an I(V) using the elastomer.

The mean full depletion voltage for Group C is 23 ± 2 V and for Group B is 22 ± 2 V. This difference is mainly due to the 2 % more doped gain layer of group C (see Table 1). The greater full depletion voltage of group A (35 ± 4 V) is related to the Epi substrate. Indeed, the Epi wafers have a substrate with lower resistivity, which translates into additional bias voltage needed to fully deplete the device in respect to the Si-Si. This is due to the different fabrication process of the Epi and Si-Si wafers. In Si-Si wafers, two silicon substrates are bonded together; one is a thick low-resistivity called handling wafer acting as a mechanical support and ohmic contact, and the other is a high resistivity (carrier wafer), which is thinned down by standard process [11]. In epitaxial wafers, a silicon crystal is grown over a thick low-resistivity handling wafer that also acts as a crystal seed for the epitaxial silicon layer grown on top of it, having a higher doping concentration with respect to Si-Si wafers. This effect was measured between a PiN strip from Wafer 1, and Wafer 5 using the experimental setup explained in 3.2. It was found that ~8 V were necessary to deplete a PiN strip from the Wafer 1 against ~0.675 V for Wafer 5. These results are in accordance with the values reported for the full depletion voltage in Fig 11.

The Breakdown Voltages are shown in Fig. 12 and were measured using the automatic procedure explained in 3.1.1. A mean breakdown voltage for good sensors measured on the backplane of about 212 V was found. Almost all the measurements with the elastomer show a higher breakdown voltage (up to 15 %) than the probe card. This difference can be associated with the procedure adopted to measure the sensor, either the probe card or the elastomer, and the number of floating strips during the measurement. Floating strips create a large electric field (producing breakdown) between themselves and the surrounding strips, meanly at the inversion layer/p-stop junction. [7]. Due to this problem given the large area of our sensors and the impossibility of properly ground all strips, the values reported for the breakdown voltage are underrated, and larger values for the breakdown voltage are expected.
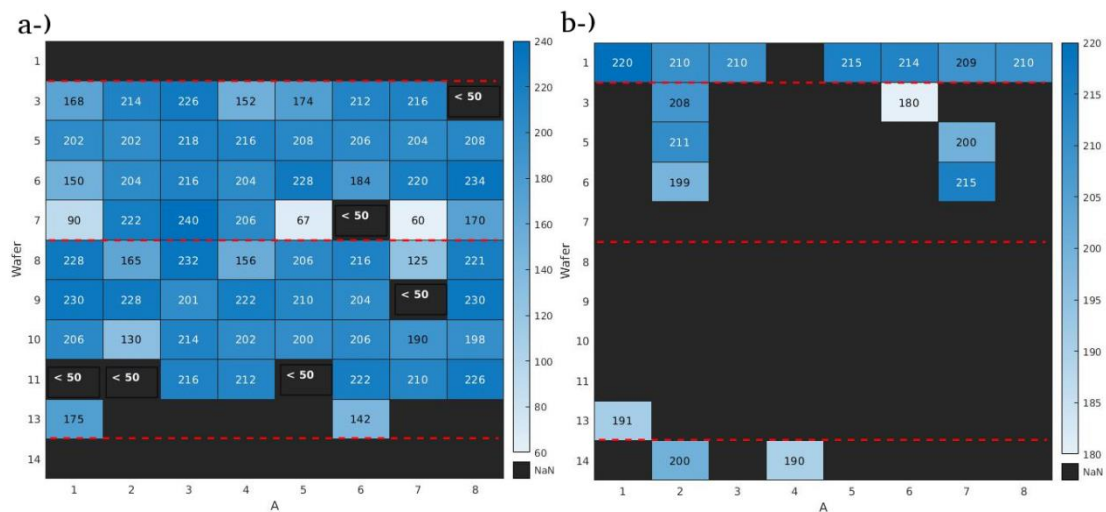

Figure 12. (a) Elastomer (b) Probe Card.

A group of 16 sensors was randomly selected, and the outcomes of the tests performed at both institutions (FBK, UNITO) were compared (see Table 4). An excellent and comparable percentage of good strips was found: 99.79 and 99.74 for the measurements performed at UNITO and FBK, respectively.

Sensor	Bad Strips (UNITO)	Bad Strips (FBK)
W1-A1,W1-A2,W1-A3, W1-A6, W1-A7,W1-A8,W3-A2,W3-A6,W5-A2,W5-A7,W6-A2,W6-A7	/	/
W1-A5	83	82,83
W13-A1	12,22,23	12,22,23
% Good Strips	99.79	99.74
% Good Sensors	87.50	87.50

Table 4.

Among the total 2336 strips measured, only one (Strip 82 of W1-A55) resulted in different measurements at FBK and UNITO. Fig 13. shows strips 81, 82, and 83 from both institutions. The probe card used at UNITO has 40 needles (24 strips were readout and the remaining strips were grounded), while the probe card of FBK has only 24 needles. The different measurements related to strip 82 can be caused by floating strips. Strip 83 has the same shape in both institutions, but it is shifted to the right in the case of UNITO. In addition, even at UNITO laboratory the strip 82 (the one "different") is moving away from strip 81 but does not fall under the criteria of bad strip.
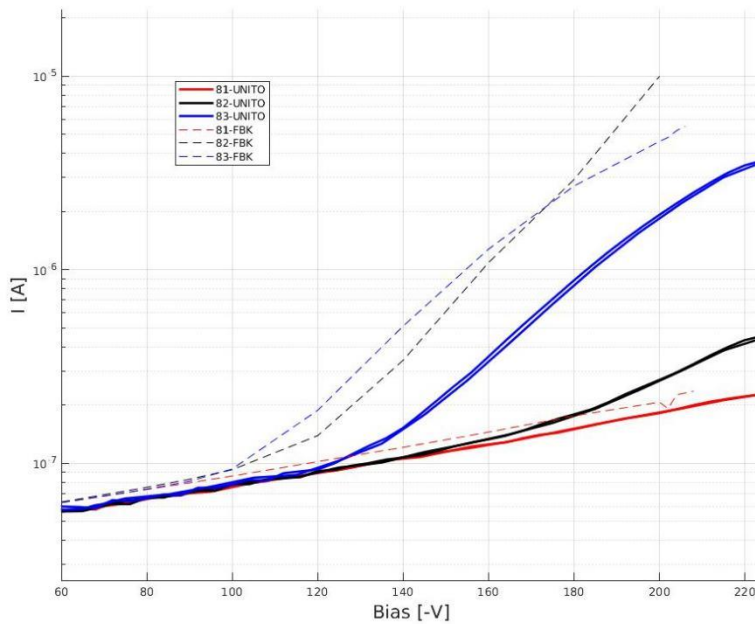

Figure 13.

5.3. Capacitance vs. Frequency, Capacitance vs. Reverse Bias Voltage, Acceptor doping concetration vs. depth

The Capacitance vs. Frequency was performed using the setup described in 3.2 to contact the strips of the sensor Type E (Fig. 1, bottom). The C(f) scan allows selecting the proper frequency of the AC signal for performing the C(V) test. The sensor type E is 1/3 part of the Bigger sensors, and it has strips with the same length and different widths (Table 5). Fig. 14 shows the C(f) scan for these detectors (Wafer 5 and Wafer 11) for partially depleted strips (Bias Voltage: - 10 V).
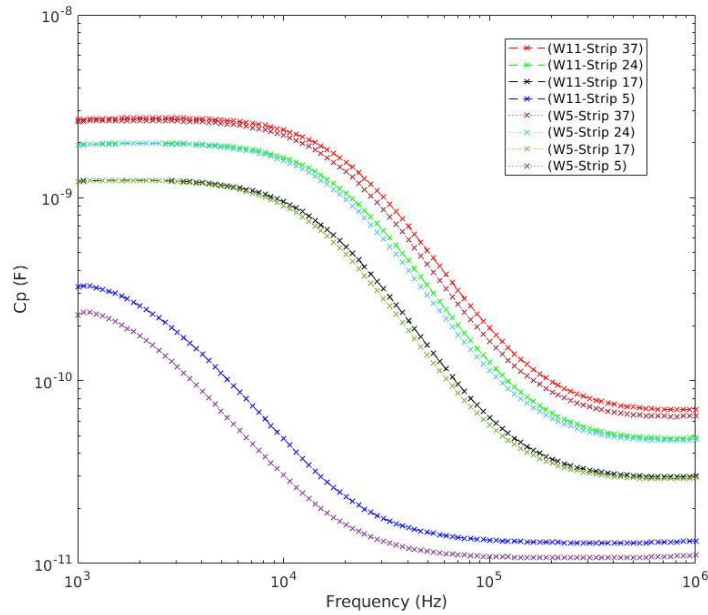
Figure 14.

Table 5. Shows the dimension of the strip of the sensor type E together with the value of frequency where started the fall-off in capacitance. The first conclusion that came out observing Table 5 and Fig. 14 is the geometry dependence of the AC signal.

Strip (Wafer)	Metal dimension (LxW)	Capacitance fall-off [Frequency (Hz)]	L/W
5 (W11,W5)	160 µm × 26260 µm	2310, 1873	164
17 (W11,W5)	340 µm × 26260 µm	2154, 2009	77
24 (W11,W5)	520 µm × 26260 µm	1747, 1629	51
37 (W11,W5)	700 µm × 26260 µm	1080, 1070	37

Table 5.

LGAD strip sensors can be modelled as a combination of resistors and capacitors, behaving like a low pass filter. The resistors represent the strips' metal, where the AC signals travel. Their value per unit length depends on the metal thickness and the width. In our case, the metal of the strips has the same length and thickness but different widths. Therefore, a small width for strip 5 results in a higher resistance than, for example, strip 37, making the AC signals drop to the ground before reaching the end of the strip. As a result, it was impossible to find a proper frequency for strip 5. An AC frequency equal to 1 kHz was selected for the other strips.

[1]https://www.technoprobe.com/
[2]https://www.prusa3d.com/category/original-prusa-i3-mk3s/
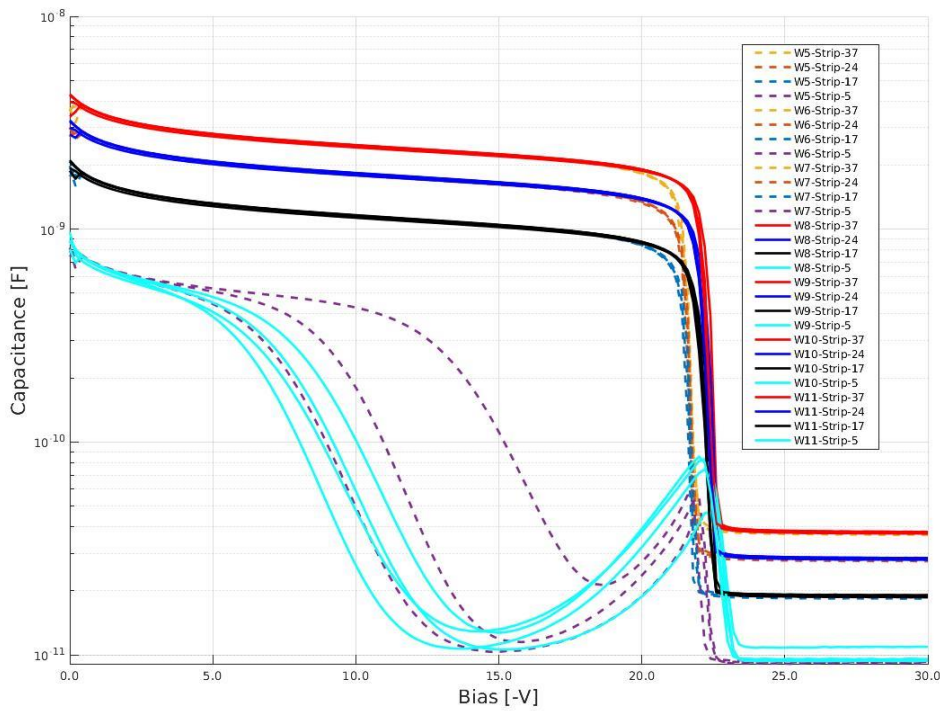[3]http://particulars.si

Figure 15.

Fig. 15 shows the Capacitance vs. Bias Voltage in semi-logarithmic scale for the selected Wafers for different strips dimension (see Table 5) measured at room temperature. The drop in capacitance corresponds to the depletion of the gain layer, calculated using the automatic procedure defined in 3.2.1. The capacitance is directly proportional to the active area of the strip and this explains the four different families of curves in Fig. 15, ranging from the one with the larger area for strip 37 in the top to the lower area for strip 5 in the bottom. The point where the capacitance remains almost constant is the full depletion voltage, which means that the high resistivity bulk is depleted. The dashed lines represent the strips from the wafers of Group B, while the solid lines are for Group C. As expected, the full depletion voltage for Group C is around 1 V higher than Group B, because of the doping concentration of the gain layer (Group C is 2 % more doped). For strip 5, the C(V) is inconsistent because of the loss of meaning and the impossibility of selecting a proper frequency. Moreover, the depletion voltage for the gain layer, the bulk, and the full depletion voltage are shown in Table 6. The obtained values are compatibles with the ones found using the I(V) curves. The bulk depletion voltage are similar for both groups because the same resistivity for the bulk were used.

Wafer	Bulk Depletion (V) from C-V (from I-V)	Full Sensor Depletion (V)
Group B	1.5 $\pm$ 0.3 (xx$\pm$xx)	22.4 $\pm$ 0.3
Group C	1.6 $\pm$ 0.4 (xx$\pm$xx)	23.0 $\pm$ 0.4

Table 6.

From the C(V) curves, one can extract the acceptor doping concentration as a function of depth, as explained by Sola in [5]. The origin of the x-axis (Fig. 16) corresponds to the n^{++}/p^+ junction. The peaks represent the gain layer implanted below the n^{++} electrode and have a doping concentration of $\sim 10^{16}\ atoms/cm^3$ in a position between 0.5-1 µm. The bulk is the flat region in the middle with a doping concentration of $10^{11} - 10^{12}\ atoms/cm^3$ for Group B and Group C. The sharp increase in doping concentration on the right is the p^{++} electrode. The reported values are compatible with the design values expected for the doping concentration after the implantation.

[1]https://www.technoprobe.com/
[2]https://www.prusa3d.com/category/original-prusa-i3-mk3s/
[3]http://particulars.si
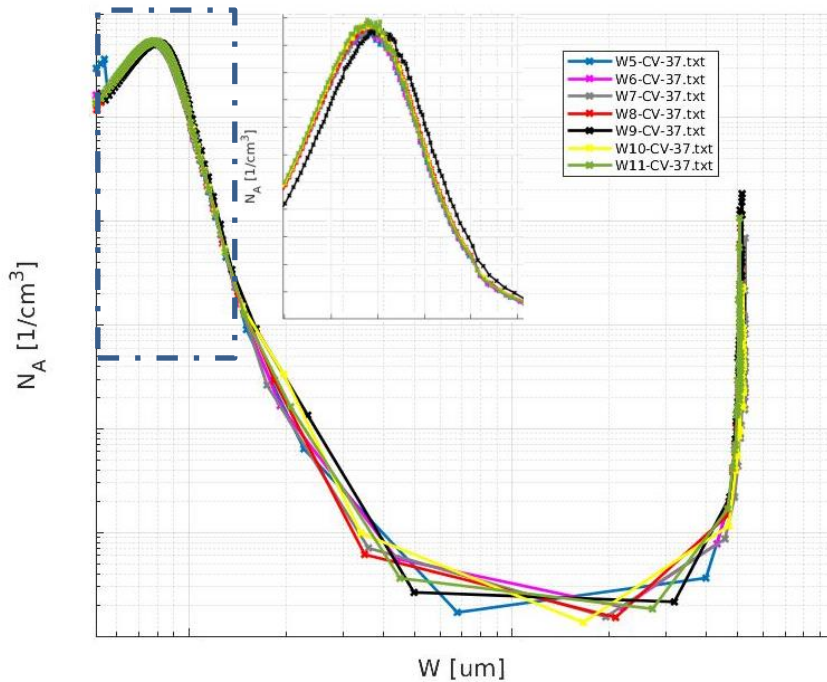
Figure 16.

Interestingly, Wafer 9 shows slightly more deep gain layer implants ($\sim$ 0.03 um) in respect to the gain implant for Wafers 8, 10, and 11. It can explain the behavior observed before in Fig. 10, where the leakage current for the Wafer 9 was 2.1 times larger than the wafers in the same group. The shift in the peak position may be due to fluctuation of the implantation energy, although this is an unlikely phenomenon, or to a variation in the dose of the n^{++} electrode. This results in a slightly shallower and less doped layer, which produces a more significant depleted distance increasing the gain and shifting the peak in the doping curve deeper in the device.

5.4. Measurements of the inter-strip distance using the TCT

The experimental setup described in 3.3 was used for measuring the inter-strip distance as a function of bias voltage and laser intensities. An infrared laser (1064 nm) with a spot of $\sim$16 μm with an attenuation of around 1 mm in Silicon emulates the behavior of charged particles crossing the detectors. In the sensors E_2, several optical windows (100 μm $\times$ 237 μm) are present in the region between two neighboring strips (strips 5 and 6), enabling laser studies in the device. The inter-strip distance was measured for three different Bias Voltages near sensors' breakdown and 4 different laser intensities to reproduce protons beam in clinics (227 MeV protons = 2 MIP; 62 MeV protons = 5 MIP). Fig 17a shows the results. The reported inter-strip distance is calculated using the distance between 50 % of the maximum of two S-curves, as shown in Fig 17b [4,7]. The different signals amplitude for each strip arises from using two different amplifiers for the two strips. It is worth saying that the inter-strip distance at the central point in the optical window along the strip was equal to 80.8 $\pm$ 0.5 μm. This value is 22 % larger than the nominal no-gain region and is due to the transition region [8]. For instance, when the e/h are generated in the periphery of the gain layer they are collected in the JTE (Fig 2c). The JTE has a gain equal to 1, as shown in Fig. 17b (knee), decreasing the effective gain region. Finally, a little dependence concerning the laser intensities (3 % for the worst case) was found for the three Bias voltages used, as shown in Fig. 17a. One of the ideas within the Medical Physics group at the University of Torino for the new generation of beam monitors is to integrate the counting [6] and timing [9,10] capabilities, which until now are separate, in the same device. To this end, several studies are lacking, such as signal delay, area, and amplitude along the strip.

[1]https://www.technoprobe.com/
[2]https://www.prusa3d.com/category/original-prusa-i3-mk3s/
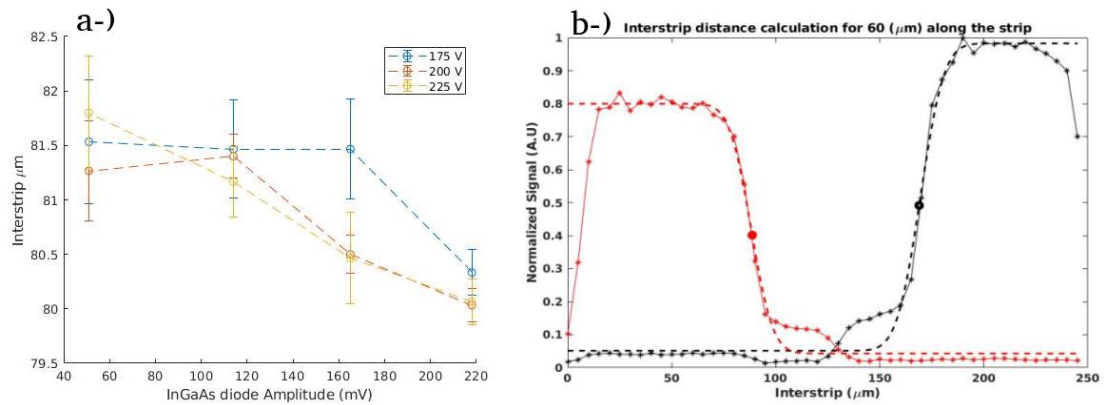[3]http://particulars.si

Figure 17.

5.6. Beam Test at CNAO

The beam test was performed at Centro Nazionale di Adroterapia Oncologica (CNAO, Pavia) with the lower energy provided by the facility (62.28 MeV). The reasons for this decision come from the fact that the average pencil beam size expressed in terms of FWHM in the air at the isocenter is maximum for lower energy, exactly 22 mm, and our two strips are placed on the edge of the detectors separately by 2.6 cm, each. Fig 18 shows the waveforms for both channels. The bias voltage used was -180 V. The value for the bias guaranteed that the multiplied holes (lower mobility) took less than 1 ns in 45 μm of active thickness [11]. We measured for both cases (PiN and LGAD) a signal duration around 2 ns, the spread on the signals is because of the limited bandwidth of the front-end electronics [11]. Observing Fig. 18a, we can distinguish that even though the proton passes across the LGAD strip, the PiN strip baseline seems to fluctuate due to this proton. The same happens when the proton passes in the PiN strip (Fig. 18b). This unavoidable effect is caused by the induced current. The latter features a bipolar shape due to the weighting-field direction changing along the path, from the readout strip to the farthest neighbor strips [16]. This can severely affect the signal whenever the gain of the sensors is not high enough to properly separate the noise from the signal.
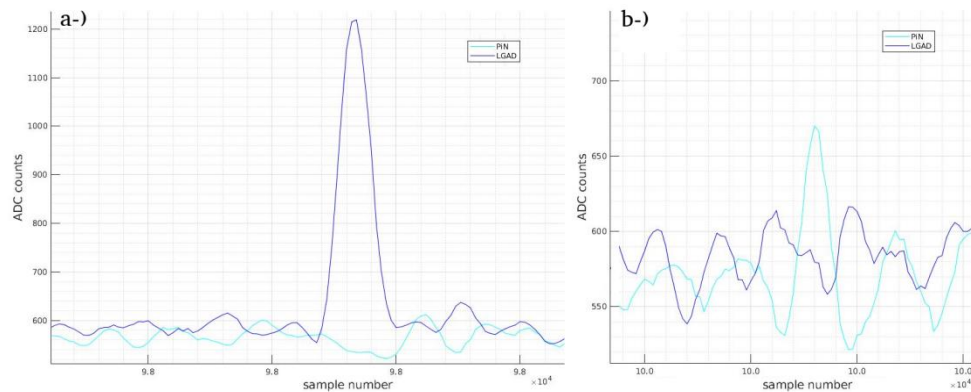

Figure 18.

For instance, Fig 19.a shows the Number of peaks vs. Peaks amplitude (ADC) for the LGAD and PiN, respectively. As shown, the LGAD strip can correctly discriminate the noise from the signal, but the amplitude of the proton signals passing in the PiN strip have the same amplitude of the signal induced from the neighboring strips (Fig. 18b and Fig. 19b). When the protons pass through the central strips, even if they are floating, a signal can be induced at the reading electrode [17], changing the baseline if many protons arrive simultaneously (Fig. 19b).
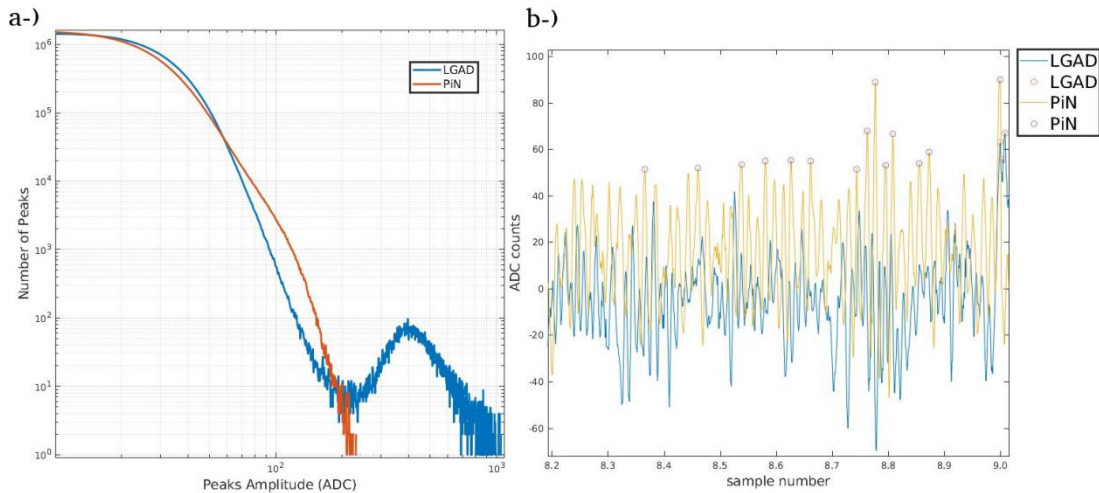
Figure 19.

Fig. 20a shows the Number of Peaks vs. Peaks Amplitude (ADC) for -180 V bias voltage for the LGAD strip. The data were fitted using a convolution between a Gaussian and Landau distribution with a coefficient of determination (R^2) equal to 0.97, giving the correct arrangement for the energy loss by protons in silicon. The reason for the Gaussian is not only to account for the electronics noise; it is known from the theory [18] that simply a Landau does not describe very well the amplitude distribution in very thin thicknesses. It should be noticed that, when the convolution between a Landau with a Gaussian distribution is performed, the maximum of the curve shifts towards larger values. Therefore, the Most Probable Value (MPV) no longer corresponds to the maximum of the curve. This is because the Landau function is asymmetric and, when it is convoluted with a symmetric (Gaussian) function, the net result is a slight shift of the distribution peak to a larger value ($\approx$ 3%). The MPV obtained from the fit is 379.5 ADC, corresponding to an amplitude of 91.08 mV. In addition, several bias voltages were applied to the detectors, and the results are shown in Fig. 20b. As expected, increasing the bias voltage, the MPV follows an exponential (R^2=0.998) trend (MPV=142.5*exp(0.00545*V)) due to the presence of the gain layer.
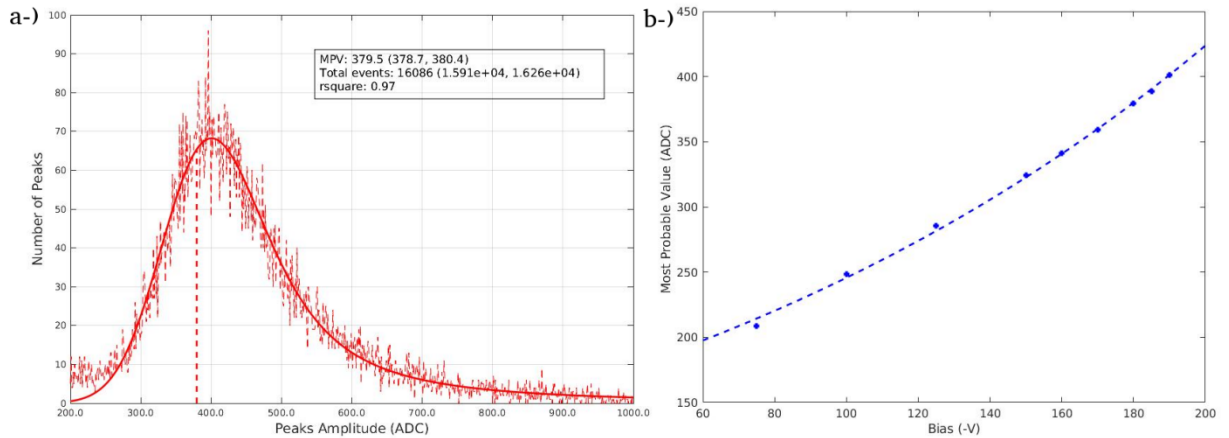

Figure 20.

6. Conclusions

A global percentage between working strips over the total number of strips measured in the entire production of 90% were found. The average full depletion voltage obtained was 22.14-23.36 V, and 34.98 V for Si-Si and Epi wafer, respectively, and a mean breakdown voltage for good sensors measured on the backplane of about 212 V were found. From selecting 16 sensors from different wafers, we found a consistent correlation between the measurements taken at FBK and at the University of Torino, where the yields were 99.74% and 99.79%, respectively. The inter-strip distance measured was $80.8 \pm 0.5\,\mu m$, 22 % larger than the

nominal no-gain distance, and has a small dependence on bias voltage or the signal amplitude. Finally, the combination between the sensor tested at CNAO and the laboratory characterization showed promising results and prepared the groundwork for future beam tests using the digital channels of the counter prototype.

Acknowledgements

References

[1] A Vignati et al., *Innovative thin silicon detectors for monitoring of therapeutic proton beams: Preliminary beam tests*, 2017 JINST 12 C12056

[2] R Sacchi et al., *Test of innovative silicon detectors for the monitoring of a therapeutic proton beam*, 2020 J. Phys.: Conf. Ser. 1662 012002

[3] Giordanengo, Simona, and Hugo Palmans. "Dose detectors, sensors, and their applications." *Medical physics* 45.11 (2018): e1051-e1072.

[4] Ferrero, Marco, et al. *An Introduction to Ultra-Fast Silicon Detectors*. CRC Press, 2021

[5] Sola, V., et al. "First FBK production of 50 μm ultra-fast silicon detectors." *Nuclear Instruments and Methods in Physics Research Section A: Accelerators, Spectrometers, Detectors and Associated Equipment* 924 (2019): 360-368.

[6] Fausti, F., et al. "A single ion discriminator ASIC prototype for particle therapy applications." *Nuclear Instruments and Methods in Physics Research Section A: Accelerators, Spectrometers, Detectors and Associated Equipment* 985 (2021): 164666.

[7] Ferrero, Marco. "Development of Ultra Fast Silicon Detector for tracking in4 dimensions". PhD Thesis. 2016.

[8] Paternoster, G., et al. "Novel strategies for fine-segmented Low Gain Avalanche Diodes." Nuclear Instruments and Methods in Physics Research Section A: Accelerators, Spectrometers, Detectors and Associated Equipment 987 (2021): 164840.

[9] Marti Villarreal, O. A., et al. "Energy measurement of clinical proton beams with a telescope of Ultra-Fast Silicon Detectors." *SIF Congress 2020*. Vol. 44. No. 143. 2021. DOI 10.1393/ncc/i2021-21143-1

[10] Vignati, A., et al. "A new detector for the beam energy measurement in proton therapy: a feasibility study." *Physics in Medicine & Biology* 65.21 (2020): 215030.

[11] Giacomini, Gabriele. "Fabrication of silicon sensors based on Low-Gain Avalanche Diodes." *Frontiers in Physics* 9 (2021): 29.

[12] Kramberger, G., "LARGE SENSOR PROBING", HGTD - MEETING, https://indico.cern.ch/event/956567/contributions/4020450/attachments/2103103/3536249/HGTD_Sensors-LargeSensorProbing.pdf

[13] Bacchetta, N., et al. "Improvement in breakdown characteristics with multiguard structures in microstrip silicon detectors for CMS." *Nuclear Instruments and Methods in Physics Research Section A: Accelerators, Spectrometers, Detectors and Associated Equipment* 461.1-3 (2001): 204-206.

[14] Fernandez M., et al. "Status report on the radiation tolerance assessment of CNM AIDA2020v2 and HPK-P2 LGADs". "16th (Virtual)" Trento" Workshop on Advanced Silicon Radiation Detectors.", 16-18/02/2021.

[15] Milanesio, Matteo. "Characterization of the Latest Ultra-Fast Silicon Detector Productions for the MIP Timing Detector of the CMS Experiment". Master Thesis://personalpages.to.infn.it/~cartigli/ufsd_project/ewExternalFiles/MatteoMilanesio_MasterThesis.pdf

[16] Spieler, Helmuth. *Semiconductor detector systems*. Vol. 12. Oxford university press, 2005.

---

[1]https://www.technoprobe.com/

[2]https://www.prusa3d.com/category/original-prusa-i3-mk3s/

[3]http://particulars.si

[17] Gatti, E., G. Padovini, and V. Radeka. "Signal evaluation in multielectrode radiation detectors by means of a time dependent weighting vector." *Nuclear Instruments and Methods in Physics Research* 193.3 (1982): 651-653.

[18] Leroy, Claude, and Pier-Giorgio Rancoita. *Principles of radiation interaction in matter and detection.* World Scientific, 2011.

[1]https://www.technoprobe.com/
[2]https://www.prusa3d.com/category/original-prusa-i3-mk3s/
[3]http://particulars.si